Journal of Power Sources 188 (2009) 606–612

Contents lists available at ScienceDirect

Journal of Power Sources

journal homepage: www.elsevier.com/locate/jpowsour

Short communication

State-of-charge estimation of lead-acid batteries using an adaptive extended Kalman filter

Jaehyun Han [a], Dongchul Kim [a], Myoungho Sunwoo [b,*]

[a] Dept. of Automotive Engineering, Graduate School, Hanyang University, 17 Haengdang-dong, Seongdong-gu, Seoul 133-791, Republic of Korea
[b] Dept. of Automotive Engineering, Hanyang University, 17 Haengdang-dong, Seongdong-gu, Seoul 133-791, Republic of Korea

ARTICLE INFO

Article history:
Received 15 October 2008
Received in revised form 17 November 2008
Accepted 24 November 2008
Available online 24 December 2008

Keywords:
Lead-acid battery
State-of-charge
Estimation
Covariance
Adaptive extended Kalman filter

ABSTRACT

Lead-acid batteries are widely used in conventional internal-combustion-engined vehicles and in some electric vehicles. In order to improve the longevity, performance, reliability, density and economics of the batteries, a precise state-of-charge (SoC) estimation is required. The Kalman filter is one of the techniques used to determine the SoC. This filter assumes an a priori knowledge of the process and measurement noise covariance values. Estimation errors can be large or even divergent when incorrect a priori covariance values are utilized. These estimation errors can be reduced by using the adaptive Kalman filter, which adaptively modifies the covariance. In this study, an adaptive extended Kalman filter (AEKF) method is used to estimate the SoC. The AEKF can reduce the SoC estimation error, making it more reliable than using a priori process and measurement noise covariance values.

1. Introduction

Lead-acid batteries, the oldest type of rechargeable battery, were invented in 1859 by the French physicist Gaston Planté [1]. Lead-acid batteries are still widely used in electrical systems, such as those employed in conventional internal-combustion-engined vehicles and some electric vehicles. In order to improve the longevity, performance, reliability, density and economics of the batteries, an accurate state-of-charge (SoC) estimation is necessary [2]. For these reasons, several methods of estimating the SoC have been developed, e.g., coulomb counting, open-circuit voltage (OCV) measurement, impedance spectroscopy, electromotive force, fuzzy logic, and the Kalman filter [1]. The Kalman filter can estimate the SoC dynamically by means of a battery model [3]. Non-linear Kalman filters, such as extended Kalman filters (EKF) [3–6] and sigma-point Kalman filters [7,8], have been applied for non-linear discrete battery models.

Generally, the Kalman filter assumes that the covariance of the process and the measurement noise are already known. Covariance values cannot, however, be identified exactly in most practical applications. Furthermore, estimation errors can be large or even diverge when an incorrect covariance is used [9]. None of the previous studies on SoC estimation has considered this covariance problem; the covariance values of the process and measurement noise are assumed to be a priori known [3–5,7,8] or determined by trial-and-error from experimental studies [6]. Nevertheless, these approaches do not provide a practical solution to the problem.

This study evaluates the use of incorrect a priori covariance values for SoC estimation using the EKF. The SoC estimation error caused by the covariance problem is reduced by adaptively modifying the covariance values with an adaptive Kalman filter [9].

2. Battery model

2.1. Battery model structure

A battery model is required in order to apply the Kalman filter to estimation of the SoC. In the present study, the zero-state hysteresis model structure was used for a discrete lead-acid non-linear battery model [4,5]. Eqs. (1) and (2) represent the zero-state hysteresis model structure.

$$\begin{aligned} s_{k+1} &= f(s_k, i_k) + w_k \\ &= s_k - \left(\frac{\eta_i T}{C}\right) i_k + w_k \end{aligned} \tag{1}$$

$$\begin{aligned} y_k &= g(s_k, i_k) + v_k \\ &= \mathrm{OCV}(s_k) + R i_k + h_k H + v_k \end{aligned} \tag{2}$$

where s is the SoC, i is the battery current, y is the battery terminal voltage, R is the battery internal resistance, H is the hysteresis value, and h is the hysteresis constant representing the sign of the

* Corresponding author. Tel.: +82 2 2290 0453; fax: +82 2 2297 5495.
E-mail addresses: wogusl@hanyang.ac.kr (J. Han), gulajima@naver.com (D. Kim), msunwoo@hanyang.ac.kr (M. Sunwoo).

0378-7753/$ – see front matter © 2008 Elsevier B.V. All rights reserved.
doi:10.1016/j.jpowsour.2008.11.143

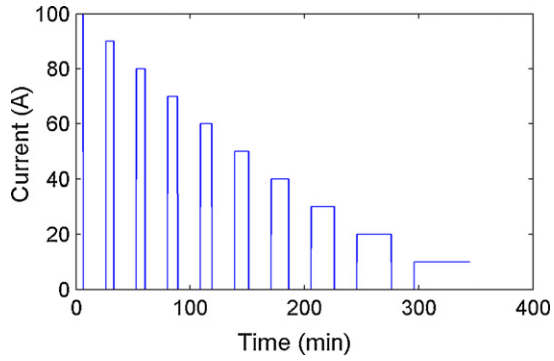

Fig. 1. Discharge current input.

hysteresis effect according to the current. For some ε sufficiently small and positive:

$$h_k = \begin{cases} -\mathrm{sgn}(i_k), & |i_k| > \varepsilon \\ h_{k-1}, & |i_k| \le \varepsilon \end{cases}. \tag{3}$$

where η_i is columbic efficiency ($\eta_i = 1$ for discharge, and $\eta_i \le 1$ for charge), T is the sampling period, and C is the nominal capacity. The parameters w and v are independent, zero-mean, Gaussian noises for the process and measurement, and their covariance values are R_w and R_v, respectively. The function $\mathrm{OCV}(s_k)$, the open-circuit voltage as a function of the SoC, can be computed as

$$\mathrm{OCV}(s_k) = K_0 + \frac{K_1}{s_k} + K_2 s_k + K_3 \ln(s_k) + K_4 \ln(1 - s_k). \tag{4}$$

2.2. Experiments

A lead-acid battery with a nominal voltage of 8 V and a nominal capacity of 100 Ah was tested. An electronic load was used at room temperature and could consume the battery current with an accuracy of ±0.3%. The battery terminal voltage and current were measured by a DAQ system from National Instruments.

The battery was tested under two different current profiles shown in Figs. 1 and 2. For each type of current profile, the battery was discharged or charged based on the constant-current pulse and rest sequences. The battery was discharged from 100 A down to 10 A. During charging, the battery was charged from 100 A down to 10 A. Positive current indicates discharge, and negative current indicates charge.

The battery terminal voltage decreased and increased with the discharge and charge current profiles, respectively. The battery terminal voltage outputs are shown in Figs. 3 and 4. Furthermore, the SoC profiles for the battery were obtained via the Ah counting method. Figs. 5 and 6 show these SoC profiles based on the discharge and charge current profiles.

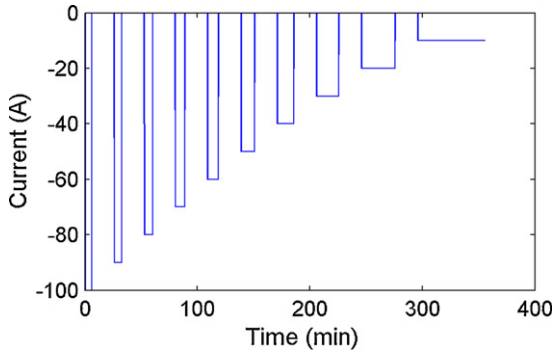

Fig. 2. Charge current input.

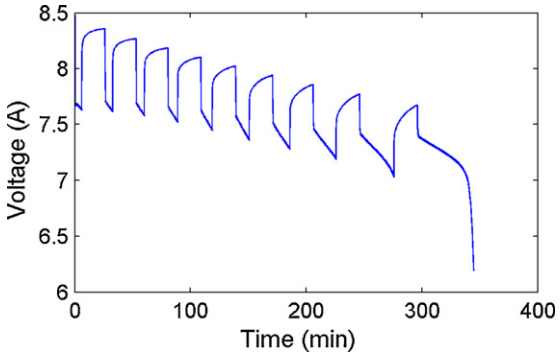

Fig. 3. Discharge voltage output.

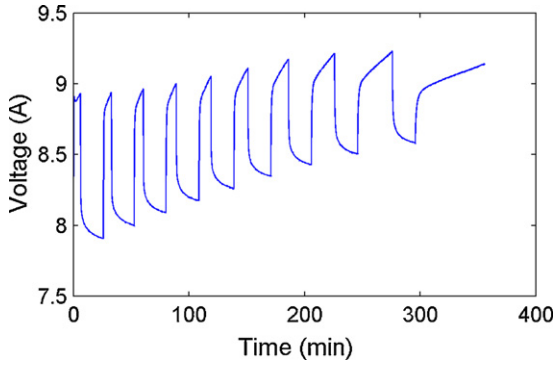

Fig. 4. Charge voltage output.

2.3. Model parameter identification

Model parameters were determined by applying the least-squares method. The battery model output equation can be represented by a regression model as expressed by

$$\begin{aligned} y_k &= g(s_k, i_k) \\ &= \mathrm{OCV}(s_k) + Ri_k + h_k H \\ &= K_0 + \frac{K_1}{s_k} + K_2 s_k + K_3 \ln(s_k) + K_4 \ln(1 - s_k) + Ri_k + h_k H \\ &= \left[1 \quad \frac{1}{s_k} \quad s_k \quad \ln(s_k) \quad \ln(1 - s_k) \quad i_k^+ \quad i_k^- \quad h_k \right] \\ &\quad \times [\, K_0 \quad K_1 \quad K_2 \quad K_3 \quad K_4 \quad R^+ \quad R^- \quad H \,]^T \\ &= \varphi_k^T \theta \end{aligned} \tag{5}$$

where i^+ and i^- are the currents for discharge and charge, respectively; i_k^+ is equal to i_k if $i_k > 0$, while i_k^- is equal to i_k if $i_k < 0$; otherwise

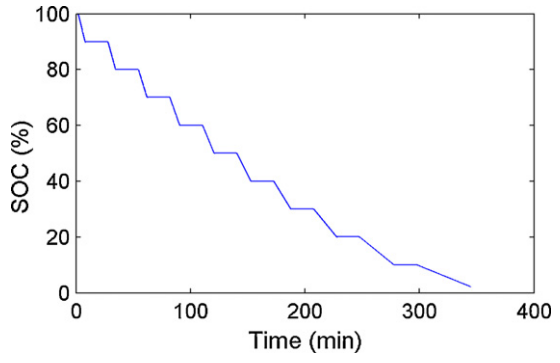

Fig. 5. Discharge SoC result.

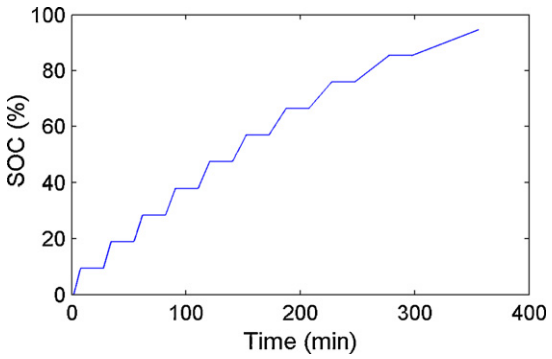

Fig. 6. Charge SoC.

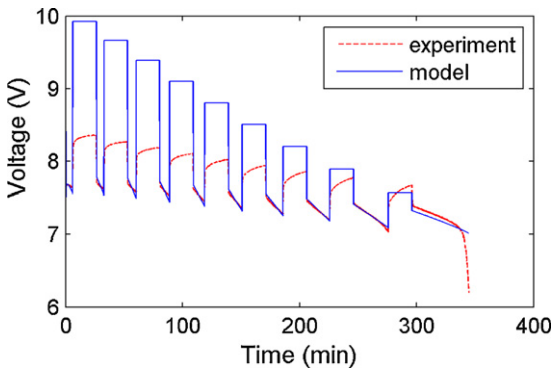

Fig. 7. Modelling result under discharge.

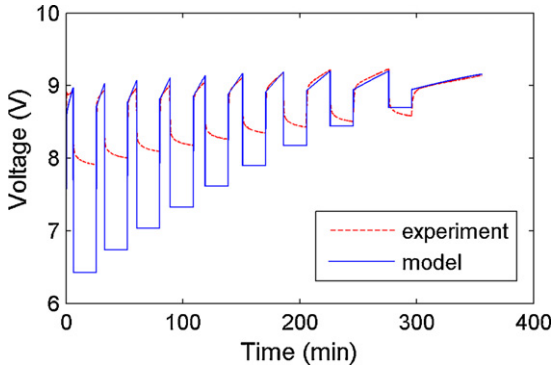

Fig. 8. Modelling result under charge.

Table 1
Modelling result of battery parameters.

K_0	6.8143
K_1	6.4382×10^{-5}
K_2	3.0301
K_3	0.045671
K_4	0.076233
R^+	-2.3626×10^{-2}
R^-	-2.5436×10^{-2}
H	−0.56082

i^+ and i^- are zero. Likewise, R^+ and R^- are the internal resistance values of the battery for discharge and charge, respectively. For N number of observations, Eq. (5) can be written as

$$Y = \Phi\theta \tag{6}$$

where $Y = [y_1, y_2, \ldots, y_N]^T$ and $\Phi = [\varphi_1^T, \varphi_2^T, \ldots, \varphi_N^T]^T$. As a result, the parameters can be obtained from $\theta = (\Phi^T\Phi)^{-1}\Phi^T Y$ for a non-singular $(\Phi^T\Phi)$. For determination of the parameters, only non-zero current observations were considered, because the zero-state hysteresis model was unable to represent the relaxation effect as a description of the time constant when the battery voltage converged to the steady-state value after a discharge or charge current was pulsed [4].

The resulting parameters are given in Table 1. Modelling of the discharge and charge using these parameters is shown in Figs. 7 and 8, respectively. The results illustrate that the battery model can represent the battery output voltages with respect to discharge and charge currents with the exception of the relaxation effect.

3. State-of-charge estimation

3.1. Extended Kalman filter

Kalman filters are widely used in estimation problems [10]. For the non-linear battery model in this study, the EKF was applied to estimate the SoC of the battery. In order to apply the EKF, the non-linear battery model in Eqs. (1) and (2) was made linear by a first-order Taylor-series expansion assuming $f(\cdot,\cdot)$ and $g(\cdot,\cdot)$ are differentiable at all operating points (s_k, i_k). Then we can obtain:

$$\begin{aligned} s_{k+1} &\approx f(\hat{s}_k^+, i_k) + A_k(s_k - \hat{s}_k^+) + w_k \\ &= A_k s_k + f(\hat{s}_k^+, i_k) - A_k\hat{s}_k^+ + w_k \end{aligned} \tag{7}$$

$$\begin{aligned} y_k &\approx g(\hat{s}_k^-, i_k) + C_k(s_k - \hat{s}_k^-) + v_k \\ &= C_k s_k + g(\hat{s}_k^-, i_k) - C_k\hat{s}_k^- + v_k \end{aligned} \tag{8}$$

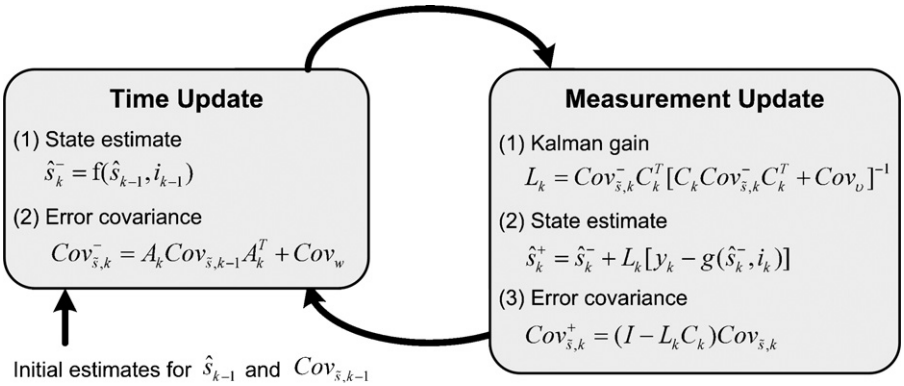

Fig. 9. Operation of extended Kalman filter.

Table 2
EKF time update equations.

$\hat{s}_k^- = f(\hat{s}_{k-1}, i_{k-1})$
$P_k^- = A_{k-1}P_{k-1}A_{k-1}^T + R_w$

Table 3
EKF measurement update equations.

$L_k = P_k^- C_k^T [C_k P_k^- C_k^T + R_v]^{-1}$
$\hat{s}_k^+ = \hat{s}_k^- + L_k[y_k - g(\hat{s}_k^-, i_k)]$
$P_k^+ = (I - L_k C_k)P_k^-$

where A_k and C_k are defined as

$$A_k = \left.\frac{\partial f(s_k, i_k)}{\partial s_k}\right|_{s_k=\hat{s}_k^+} \tag{9}$$

$$C_k = \left.\frac{\partial g(s_k, i_k)}{\partial s_k}\right|_{s_k=\hat{s}_k^-} \tag{10}$$

The operation of the EKF is shown in Fig. 9 [11,12]. First, the initial state and error covariance values are determined. Then, the covariance values are predicted using the model. After that, the state and error covariance values are corrected using the output measurement. The prediction and correction sequence was repeated every time step except when the battery current was zero. The equations describing the operation of the EKF are presented in Tables 2 and 3.

From the battery model in Eqs. (7) and (8), the EKF time and measurement update equations can be computed as follows:

$$\hat{s}_k^- = \hat{s}_{k-1}^+ - \left(\frac{\eta_i T}{C}\right) i_{k-1} \tag{11}$$

$$P_k^- = P_{k-1} + R_w \tag{12}$$

$$L_k = P_k^- C_k^T [C_k P_k^- C_k^T + R_v]^{-1} \tag{13}$$

$$C_k = -\frac{K_1}{(\hat{s}^-)^2} + K_2 + \frac{K_3}{\hat{s}_k^-} - \frac{K_4}{1-\hat{s}_k^-} \tag{14}$$

$$\hat{s}_k^+ = \hat{s}_k^- + L_k \times \left[y_k - (K_0 + \frac{K_1}{\hat{s}_k^-} + K_2\hat{s}_k^- + K_3\ \ln(\hat{s}_k^-) + K_4 \ln(1-\hat{s}_k^-) + Ri_k + h_k H)\right] \tag{15}$$

$$P_k^+ = (I - L_k C_k)P_k^- \tag{16}$$

3.1.1. State-of-charge estimation results using EKF

The SoC of the battery was estimated from the experimental data and the EKF model. The initial values of the state and error covariance, the process noise covariance, and the measurement noise covariance used in the estimation are shown in Table 4. The SoC estimation results are presented in Figs. 10 and 11. In Figs. 12 and 13, the SoC estimation errors are shown to converge into a ±5% error band.

Table 4
Simulation conditions of SoC estimation.

$\hat{s}_0$	50%
P_0	1
R_w	1
R_v	1

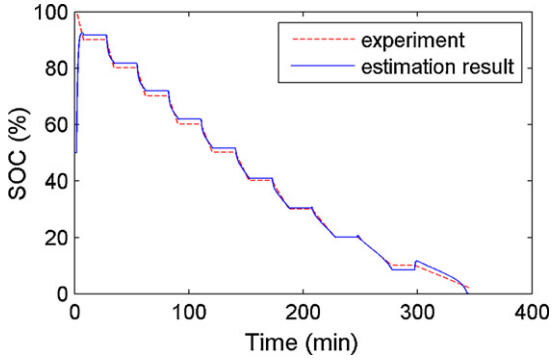

Fig. 10. SoC estimation under discharge using EKF.

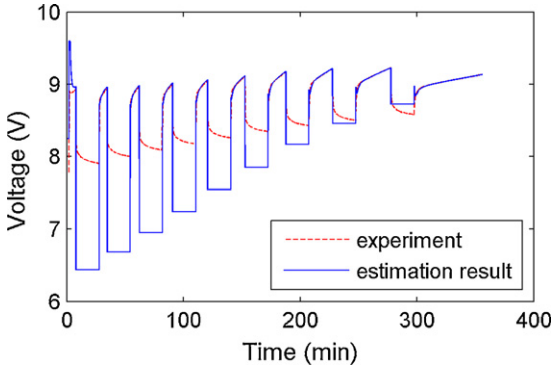

Fig. 11. SoC estimation under charge using EKF.

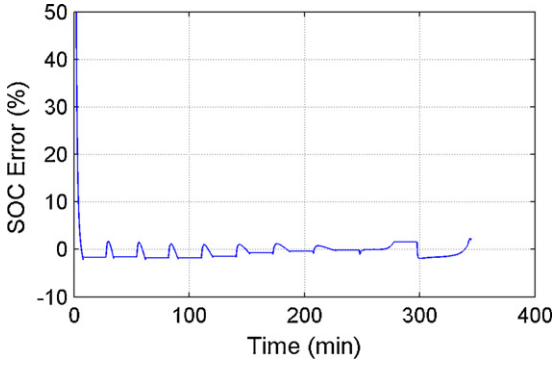

Fig. 12. SoC estimation error under discharge using EKF.

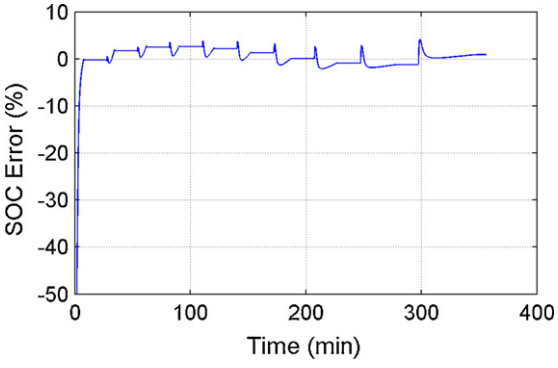

Fig. 13. SoC estimation error under charge using EKF.

3.2. Adaptive extended Kalman filter (AEKF)

A Kalman filter basically assumes that the covariance of both the process and the measurement noise are known; assumed covariance values were used in Section 3.1.1. These covariance values cannot, however, be precisely known. Moreover, improper covariance values can result in large or divergent estimation errors. Thus, in practice, these covariance values are often used as design parameters [13]. Otherwise, the covariance values can be estimated to improve the performance of the Kalman filter by employing an adaptive Kalman filter. Mehra [9] classified adaptive Kalman filter methods into four categories: Bayesian, maximum likelihood, correlation, and covariance matching. These adaptive Kalman filter methods have been applied to other applications, including an inertial navigation system and a global positioning system [14,15]. In this section, an AEKF employing the covariance matching approach was applied to battery SoC estimation. The results obtained using the AEKF were compared with the SoC estimation results obtained using the EKF in Section 3.1.

In the covariance matching method, the innovations sequence, which is a function of previous observations and state estimates, is defined as

$$z_k = y_k - g(\hat{s}_k^-, i_k) \tag{17}$$

Substituting the output model, Eq. (8), into (17), this innovation sequence can be written as

$$\begin{aligned} z_k &\approx g(\hat{s}_k^-, i_k) + C_k(s_k - \hat{s}_k^-) - g(\hat{s}_k^-, i_k) + v_k \\ &= C_k(s_k - \hat{s}_k^-) + v_k \end{aligned} \tag{18}$$

From this innovation sequence, the theoretical covariance can be obtained by taking the variance on both sides of Eq. (18):

$$R_{z_k} = C_k P_k^- C_k^T + R_{v_k} \tag{19}$$

Then, an estimate of R_{v_k} can be obtained from $\hat{R}_{z_k}$, which is the statistical sample variance estimate of R_{z_k}:

$$\hat{R}_{v_k} = \hat{R}_{z_k} - C_k P_k^- C_k^T \tag{20}$$

where $\hat{R}_{z_k}$ can be computed by averaging inside a moving estimation window of size N as follows:

$$\hat{R}_{z_k} = \frac{1}{N}\sum_{i=i_0}^{k} z_i z_i^T \tag{21}$$

where $i_0 = k - N + 1$ is the first sample inside the estimation window.

Likewise, for an estimate of R_{w_k}, the process noise, w_k, can be computed from Eq. (7), subtracting Eq. (11) as shown:

$$w_k = s_{k+1} - \hat{s}_{k+1}^- - s_k + \hat{s}_k \tag{22}$$

This noise can be transformed as

$$w_k = \tilde{s}_{k+1} - \tilde{s}_k + \Delta s_{k+1} \tag{23}$$

where $\Delta s_{k+1} = \hat{s}_{k+1} - \hat{s}_{k+1}^-$. Then, the theoretical process noise covariance can be obtained from:

$$R_{w_k} = P_{k+1} - P_k + R_{\Delta s_{k+1}} \tag{24}$$

As a result, an estimate of R_{w_k} can be computed from the statistical sample variance estimate of $R_{\Delta s_{k+1}}$ as follows:

$$\hat{R}_{w_k} = P_{k+1} - P_k + \frac{1}{N}\sum_{j=j_0}^{k} \Delta s_j \ \Delta s_j^T \tag{25}$$

This can be approximated by substituting $\Delta s_k = L_k z_k$ and $\hat{R}_{z_k}$ into Eqs. (15) and (21), respectively, to obtain:

$$\hat{R}_{w_k} \approx L_k \hat{R}_{z_k} L_k^T \tag{26}$$

3.2.1. State-of-charge estimation results using AEKF

The same initial values that were used for the state, the state error covariance, the process noise covariance, and the measurement noise covariance in the EKF estimation were also used for the

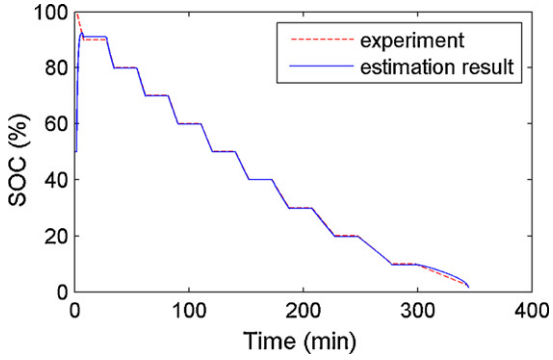

Fig. 14. SoC estimation under discharge using AEKF.

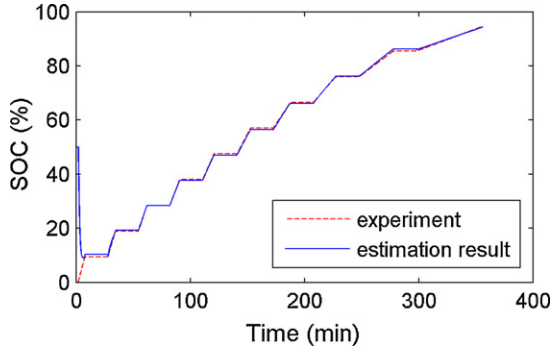

Fig. 15. SoC estimation under charge using AEKF.

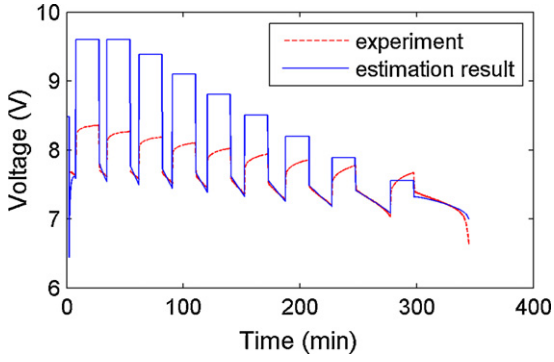

Fig. 16. Battery terminal voltage estimation result under discharge using AEKF.

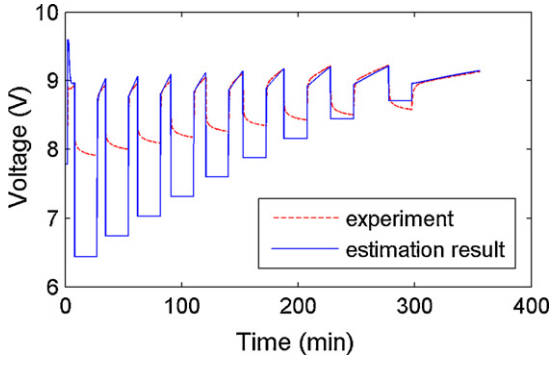

Fig. 17. Battery terminal voltage estimation under charge using AEKF.

AEKF estimation. These values are shown in Table 4. It is important to note that the two values for the process and measurement noise covariance were adapted using Eqs. (20) and (26). The SoC estimation results are presented in Figs. 14–17. The SOC estimation errors in Figs. 18 and 19 converge into about a ±1% error band. Figs. 20 and 21 show the difference between the average SoC estimation errors for the EKF and the AEKF. The figures show that the AEKF results in smaller average SoC estimation errors than does the EKF for the entire estimation time. The average SoC estimation error is computed as follows:

$$\tilde{s}_{\mathrm{av},k} = \frac{1}{k+1}\sum_{j=0}^{k}|\tilde{s}_j| \tag{27}$$

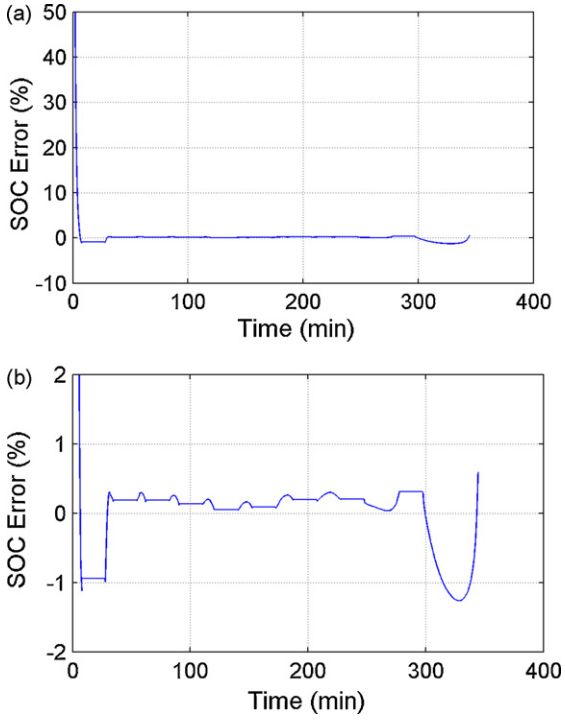

Fig. 18. SoC estimation error under discharge using AEKF; (a) whole view and (b) enlarged view.

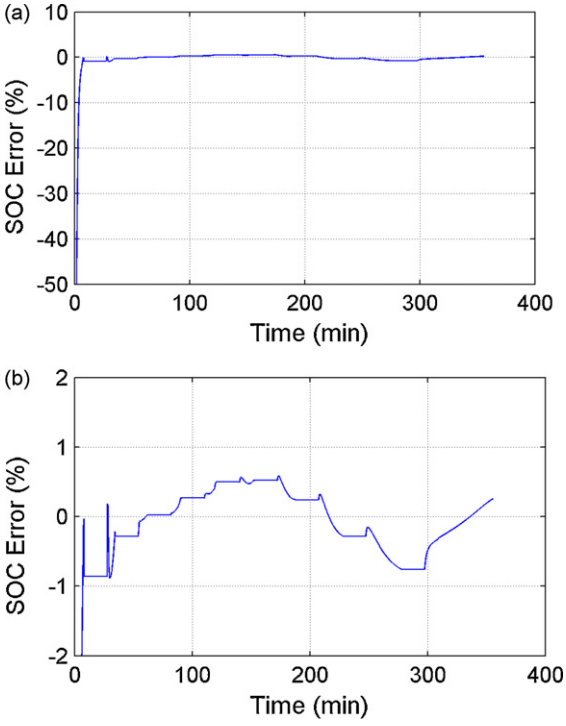

Fig. 19. SoC estimation error under charge using AEKF; (a) whole view and (b) enlarged view.

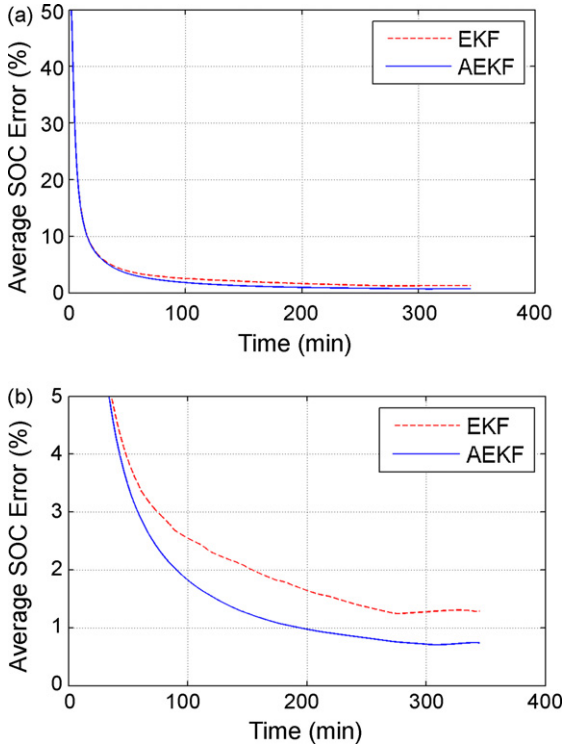

Fig. 20. Average SoC estimation errors under discharge using EKF and AEKF; (a) whole view and (b) enlarged view.

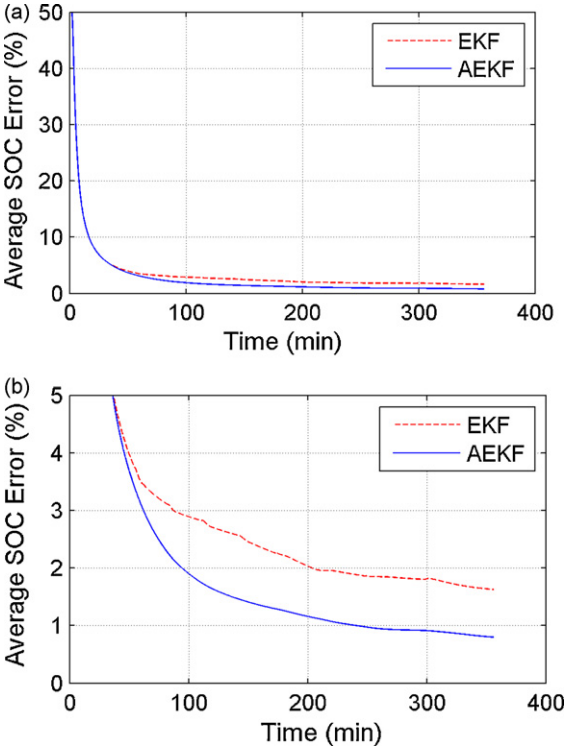

Fig. 21. Average SoC estimation errors under charge using EKF and AEKF; (a) whole view and (b) enlarged view.

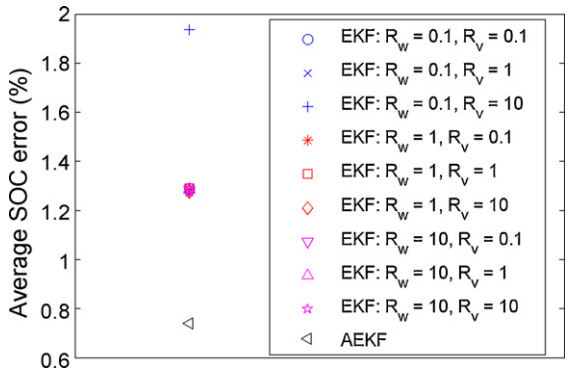

Fig. 22. Comparison of the average SoC estimation errors under discharge using EKF with several covariance values and AEKF.

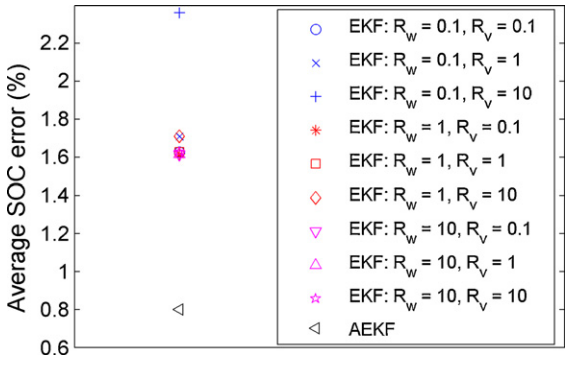

Fig. 23. Comparison of average SOC estimation errors under charge using EKF with several covariance values and AEKF.

Moreover, in order to obtain the effect of the process and measurement noise covariance values on the EKF estimation, nine sets of process and measurement covariance values are applied to the SOC estimation. In Figs. 22 and 23, the average SoC estimation errors for all nine sets of covariance values are compared with the estimation errors obtained when using the AEKF. The AEKF results exhibit smaller average SoC errors than do the EKF results for all nine sets of covariance values.

4. Conclusions

In this study, the SoC of a lead-acid battery is estimated using the AEKF. The SoC estimation results obtained from the AEKF are compared with those obtained from the EKF. The AEKF results exhibit a smaller SoC estimation error than do the EKF, because the AEKF can also estimate the process and measurement noise covariance values which can lead to large or even divergent estimation errors. Hence, the AEKF can reduce the SoC estimation error when working with unknown process and measurement noise covariance values.

Acknowledgements

The research was financially supported by the Ministry of Knowledge Economy (MKE) and Korea Industrial Technology Foundation (KOTEF) through the Human Resource Training Project for Strategic Technology, and also partially supported by the Brain Korea 21 Project in 2008.

References

[1] V. Pop, H.J. Bergveld, P.H.L. Notten, P.P.L. Regtien, Meas. Sci. Technol. 16 (2005) R93–R110.
[2] G.L. Plett, J. Power Sources 134 (2004) 252–261.
[3] S. Piller, M. Perrin, A. Jossen, J. Power Sources 96 (2001) 113–120.
[4] G.L. Plett, J. Power Sources 134 (2004) 262–276.
[5] G.L. Plett, J. Power Sources 134 (2004) 277–292.
[6] A. Vasebi, M. Partovibakhsh, S.M.T. Bathaee, J. Power Sources 161 (2007) 1369–1384.
[7] G.L. Plett, J. Power Sources 161 (2006) 1356–1368.
[8] G.L. Plett, J. Power Sources 161 (2006) 1369–1384.
[9] R.K. Mehra, IEEE Trans. Autom. Control 17 (1972) 693–698.
[10] R.E. Kalman, Trans. ASME 82 (1960) 35–45.
[11] M.S. Grewal, A.P. Andrews, Kalman Filtering: Theory and Practice using MATLAB, second ed., John Wiley & Sons, New York, 2001.
[12] S. Haykin, Kalman Filtering and Neural Networks, John Wiley & Sons, New York, 2001.
[13] G.F. Franklin, J.D. Powell, M. Workman, Digital Control of Dynamic Systems, third ed., Addison Wesley, 1998, pp. 389–394.
[14] D. Jwo, H. Huang, IEEE Int. Conf. Syst. Man Cybern. 4 (2005) 3859–3865.
[15] A.H. Mohamed, K.P. Schwarz, J. Geodesy 73 (4) (1999) 193–203.